0090-9556/11/3910-1883–1894$25.00
DRUG METABOLISM AND DISPOSITION
Vol. 39, No. 10
40980/3717905
Printed in U.S.A.

DMD 39:1883–1894, 2011

In Vitro and In Vivo Metabolism of a Selective δ-Opioid Receptor

Jian Guo, Chungang Gu, Diansong Zhou, Charles S. Elmore, Khanh H. Bui, and Scott W. Grimm

Clinical Pharmacology and DMPK (J.G., C.G., D.Z., K.H.B., S.W.G.) and Chemistry (C.S.E.), AstraZeneca Pharmaceuticals, Wilmington, Delaware

Received June 2, 2011; accepted July 13, 2011

ABSTRACT:

4-({4-[(2-Hydroxy-ethyl)-methyl-carbamoyl]-phenyl}-quinolin-8-yl-methylene)-1-thiazol-4-ylmethyl-piperidinium (compound I) is a selective agonist of δ-opioid receptor developed for the treatment of depressive and anxiety disorders. The in vitro biotransformation studies using rat, dog, and human hepatocytes showed that the metabolites detected in human hepatocytes were also found in either rat or dog hepatocytes. M1 (N-dealkylation), M2 (N-demethylation), and M4 (carboxylic acid metabolite) were major phase I metabolites observed in all three species. Human CYP3A4/5 isoenzymes were identified to be the primary enzymes responsible for the formation of M1 and M2 in human liver microsomes. After single oral administration of [^{14}C]compound I, the major elimination route for [^{14}C]compound I and its metabolites in rat was through feces with 92.9% recovery. The results from the bile duct-cannulated study revealed that a minimum of 51% of administered dose was absorbed in rats. The pharmacokinetic analysis using unlabeled parent drug showed that compound I was rapidly absorbed and exhibited a mean apparent terminal half-life of approximately 2.7 h. A total of 15 metabolites of compound I were detected and profiled in rat urine, bile, and feces. In rat bile, compound I accounted for <1.5% of the excreted dose, suggesting that compound I underwent extensive metabolism before elimination. The structures of metabolites were elucidated by high-resolution tandem mass spectrometry. M1, M4, and M6 were the most abundant metabolites observed in rat bile. Only a low level of parent [^{14}C]compound I was observed in rat plasma.

Introduction

Major depressive disorder is a psychiatric disorder characterized by the presence of one or more depressive episodes without a history of manic, mixed, or hypomanic episodes. The typical antidepressant treatments increase neurotransmitter signaling by preventing reuptake into presynaptic terminals. The most frequently used antidepressants include selective serotonin reuptake inhibitors, norepinephrine reuptake inhibitors, dopamine reuptake inhibitors, or reuptake blockers at multiple neurotransmitters (Burrows et al., 1998; Hajós et al., 2004; Jutkiewicz, 2006; Papakostas et al., 2008).

In several studies, the opioid receptors were proposed as a novel target system for the treatment of depression and anxiety (Nieto et al., 2005; Jutkiewicz et al., 2006; Saitoh et al., 2008). Opioid receptors are a family of G protein-coupled receptors and are classified as δ, μ, and κ receptors, according to the endogenous opioid peptides, namely the endorphins, enkephalins, and dynorphin, respectively (Raynor et al., 1994). Evidence from animal studies has shown that the inhibitor of the catabolism of enkephalins exhibits antidepressant effects on the learned helplessness model in the rat (Tejedor-Real et al., 1998). It has been reported that δ-opioid receptor-deficient mice displayed altered emotional responses that are consistent with a depressive-like profile of behaviors (Filliol et al., 2000). Moreover, the δ-opioid receptor (DOR) agonists have been shown to have antidepressant-like properties in several animal models (Broom et al., 2002; Torregrossa et al., 2006; Aguila et al., 2007; Vergura et al., 2008). The antidepressant-like effects of the nonpeptidic δ-opioid agonists were blocked by the selective DOR antagonist naltrindole (Torregrossa et al., 2004). Preclinical studies also demonstrated that δ-opioid receptors were involved in regulation of anxiety-like behaviors. In particular, the administration of (+)-4-[(α*R*)-α-((2*S*,5*R*)-4-allyl-2,5-dimethyl-1-piperazinyl)-3-methoxybenzyl]-*N*,*N*-diethylbenzamide (SNC80), a selective DOR agonist, was associated with anxiolytic-like effects, whereas selective DOR antagonists, such as naltrindole, produce anxiogenic-like behaviors in animal models (Saitoh et al., 2004, 2005; Perrine et al., 2006). Of importance, although the toxicities associated with opioids are significant and include respiratory depression, constipation, and risk of abuse or addiction, these toxicities are attributed predominantly to the μ-opioid receptor but not the δ-opioid receptor (Bausch et al., 2005). Tolerance was not observed after chronic administration of the selective δ-opioid receptor agonist (Aguila et al., 2007). These findings have fueled an increased intensity to develop selective δ-opioid agonists for potential use as antidepressants and anxiolytic agents devoid of adverse side effects.

4-({4-[(2-Hydroxy-ethyl)-methyl-carbamoyl]-phenyl}-quinolin-8-yl-methylene)-1-thiazol-4-ylmethyl-piperidinium (compound I) (Fig. 1) is a

Article, publication date, and citation information can be found at http://dmd.aspetjournals.org.
doi:10.1124/dmd.111.040980.

ABBREVIATIONS: DOR, δ-opioid receptor; SNC80, (+)-4-[(α*R*)-α-((2*S*,5*R*)-4-allyl-2,5-dimethyl-1-piperazinyl)-3-methoxybenzyl]-*N*,*N*-diethylbenzamide; compound I, 4-({4-[(2-hydroxy-ethyl)-methyl-carbamoyl]-phenyl}-quinolin-8-yl-methylene)-1-thiazol-4-ylmethyl-piperidinium; BDC, bile duct-cannulated; P450, cytochrome P450; HPLC, high-performance liquid chromatography; DMSO, dimethyl sulfoxide; HLM, human liver microsomes; LC, liquid chromatography; MS/MS, tandem mass spectrometry; TRA, total radioactivity; LC-MS, liquid chromatography-mass spectrometry; CID, collision-induced dissociation; MRM, multiple reaction monitoring; MS, mass spectrometry.

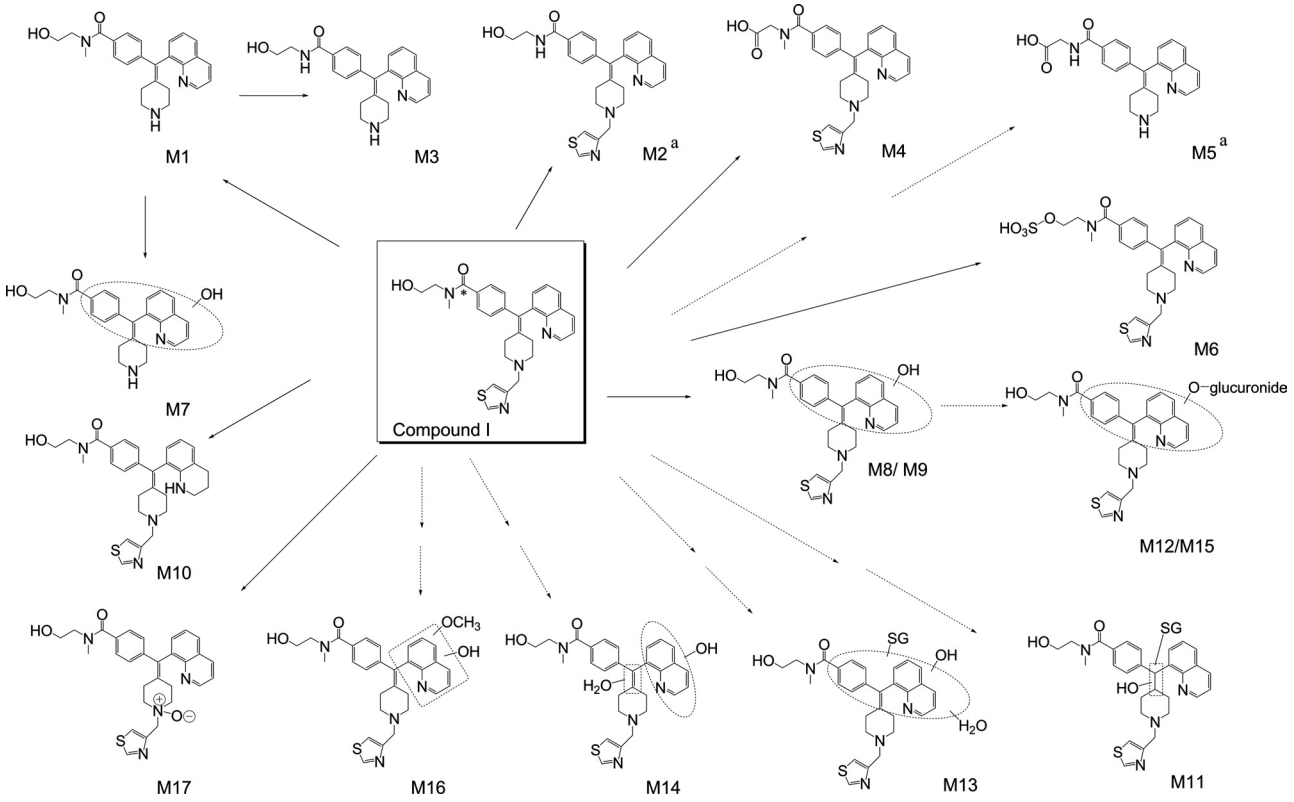

FIG. 1. Proposed biotransformation pathway of [^{14}C]compound I. *, position of ^{14}C on compound I. a, metabolites only observed in vitro.

selective agonist at the δ-opioid receptor developed for the treatment of depressive and anxiety disorders. The objectives of the present study were to investigate the in vitro metabolism of [^{14}C]compound I in hepatocytes from rat, dog, and human and absorption, excretion, and metabolism of [^{14}C]compound I in intact and bile duct-cannulated (BDC) rats to support its toxicological evaluation. The cytochrome P450 isoenzymes responsible for the formation of two major metabolites in human hepatocytes were examined using recombinant human cytochrome P450 enzymes and selective chemical inhibitors of corresponding enzymes.

Materials and Methods

Chemicals. [^{14}C]Compound I (>99% radiochemical purity), authentic standard of M1 *N*-(2-hydroxyethyl)-*N*-methyl-4-(piperidin-4-ylidene(quinolin-8-yl)methyl)benzamide, M2 (*N*-(2-hydroxyethyl)-4-(quinolin-8-yl(1-(thiazol-4-ylmethyl)piperidin-4-ylidene)methyl)-benzamide), M1-d_6, M2-d_4, and compound I-d_4 were synthesized at AstraZeneca Pharmaceuticals (Wilmington, DE). HPLC-grade solvents were purchased from Thermo Fisher Scientific (Waltham, MA). All other chemicals were purchased from Sigma-Aldrich (St. Louis, MO). Human cDNA-expressed enzymes were purchased from BD Gentest (Woburn, MA). Male Wistar Han rat cryopreserved hepatocytes were purchased from XenoTech, LLC (Kansas City, KS). Male beagle dog cryopreserved hepatocytes were purchased from CellzDirect (Durham, NC). Human cryopreserved hepatocytes (from three donors) were purchased from BD Gentest. Pooled human liver microsomes were purchased from BD Gentest.

Synthesis of Metabolite Standards. *Preparation of N-(2-hydroxyethyl)-N-methyl-4-(piperidin-4-ylidene(quinolin-8-yl)methyl)benzamide (M1).* An impure sample of *N*-(2-hydroxyethyl)-*N*-methyl-4-(piperidin-4-ylidene(quinolin-8-yl) methyl)benzamide (1 g, 33% UV area % purity) was purified via reverse-phase HPLC on a Gemini NX C18 HPLC column (30 × 100 mm) using water with 0.1 M NH_4HCO_3 buffer (pH 10) and acetonitrile to give 139 mg of the target compound as a white solid. ^{1}H NMR (500 MHz, DMSO-d_6) δ ppm 1.82 (m, 2H), 2.30 (m, 2H), 2.59 (m, 1H), 2.68 (m, 1H), 2.76 (m, 1H), 2.84 (m, 1H), 2.93 (br s, 3H), 3.17 (m, 2H), 3.45 (m, 3H), 4.71 (br s, 1H), 7.25 (m, 2H), 7.33 (m, 2H), 7.49 (dd, J = 8.2, 4.3 Hz, 1H), 7.59 (m, 2H), 7.88 (m, 1H), 8.33 (dd, J = 8.2, 1.8 Hz, 1H), 8.91 (dd, J = 4.1, 1.7 Hz, 1H). High-resolution mass spectrometry measured for $C_{25}H_{28}O_2N_3$, $[M+H]^+$ at *m/z* 402.2169 (calculated: 402.2176).

Preparation of N-(2-hydroxyethyl)-4-(quinolin-8-yl(1-(thiazol-4-ylmethyl) piperidin-4-ylidene)methyl)benzamide (M2). A solution of 248 mg (0.49 mmol) of morpholino(4-(quinolin-8-yl(1-(thiazol-4-ylmethyl)piperidin-4-ylidene)methyl) phenyl)methanone in 15 ml of 6 M HCl was purged with N_2 and heated in a sealed tube at 105°C overnight. The solvent was removed at reduced pressure to give 250 mg of the target compounds as a brown solid. The product, 4-(quinolin-8-yl(1-(thiazol-4-ylmethyl)piperidin-4-ylidene)methyl)benzoic acid, was used in the next reaction without further purification. A slurry of 250 mg (0.49 mmol) of 4-(quinolin-8-yl(1-(thiazol-4-ylmethyl)piperidin-4-ylidene)methyl)benzoic acid in 3.5 ml of dimethylformamide was stirred at room temperature as 1.33 g (3.49 mmol) of *O*-(7-azabenzotriazol-1-yl)-*N,N,N′,N′*-tetramethyluronium hexafluorophosphate was added. The resulting solution was stirred for 5 min, and then 1.0 ml (17 mmol) of ethanolamine was added. The reaction was stirred for 2 h and then was diluted with 10 ml of water. The resulting mixture was extracted 4 times with 5 ml of $CHCl_3$, and the combined organic extracts were dried ($MgSO_4$). The sample was concentrated to dryness and purified by reverse-phase HPLC to give 136 mg of the target compound as a white powder. ^{1}H NMR (500 MHz, DMSO-d_6) δ ppm 1.92 (dd, J = 8.1, 4.1 Hz, 1H), 2.00 (m, 1H), 2.37 (m, 3H), 2.5 (m, ~2H, overlapping with solvent), 2.63 (m, 1H), 3.27 (m, 2H), 3.46 (q, J = 6.2Hz, 2 H), 3.67 (s, 2H), 4.62 (t, J = 5.6 Hz, 1H), 7.32 (d, J = 8.2 Hz, 2H), 7.48 (m, 2H), 7.58 (m, 2H), 7.69 (d, J = 8.2 Hz, 2H), 7.88 (m, 1H), 8.23 (t, J = 5.6 Hz, 1H), 8.32 (dd, J = 8.2, 1.5 Hz, 1H), 8.87 (dd, J = 4.1, 1.7 Hz, 1H), 9.01 (d, J = 1.8 Hz, 1H). High-resolution mass spectrometry measured for $C_{28}H_{29}O_2N_4S$, $[M + H]^+$ found at *m/z* 485.1989 (calculated *m/z* 485.2006).

Hepatocyte Incubations. Human, rat, or dog cryopreserved hepatocytes were thawed and prepared in Williams' E buffer (pH = 7.4) containing 2 mM glutamine, insulin transferrin selenium mixtures, and 25 mM HEPES. The initial viability of the hepatocytes from rat, dog, and human was more than 90%. Approximately 2 million viable cells in a 1-ml suspension were incubated with [^{14}C]compound I (specific activity approximately 30 mCi/mmol) at 10 and 50 μM for 2 h at 37°C. The incubation was terminated by addition of 2 volumes of acetonitrile. The resulting mixtures were centrifuged to remove

cellular debris. The solvent in aliquots of 1.2 ml of supernatant was evaporated to dryness. The residues were reconstituted into 0.4 ml of the initial mobile phase used in the HPLC analysis. The hepatocyte incubations that were quenched after spiking with the test compound in the medium were used as negative controls.

Identification of P450 Enzymes Responsible for the Metabolism of Compound I. The formation of M1 and M2 in pooled HLM was conducted under linear conditions with respect to incubation time and microsomal protein concentrations. All incubations were performed at 37°C for 20 min. The incubation mixture contained 3 μM compound I, 0.2 mg/ml HLM, 5 mM $MgCl_2$, and 0.1 M potassium phosphate buffer (pH 7.4) in a total volume of 0.2 ml, either alone or with selective P450 inhibitors. Chemical inhibitors consisted of furafylline (2 and 10 μM), tranylcypromine (1 and 5 μM), ticlopidine (1 and 5 μM), montelukast (0.2 and 1 μM), sulfaphenazole (1 and 5 μM), (+)-*N*-3-benzylnirvanol (1 and 5 μM), quinidine (0.2 and 1 μM), or ketoconazole (0.2 and 1 μM), which selectively inhibit CYP1A2, CYP2A6, CYP2B6, CYP2C8, CYP2C9, CYP2C19, CYP2D6, or CYP3A, respectively. The reactions were started by the addition of 1 mM NADPH. Furafylline was preincubated with HLM and NADPH for 15 min to increase its inhibitory effect on CYP1A2. Reactions were terminated by the addition of 2 volumes of acetonitrile. After centrifugation, the supernatant was extracted using an automated solid-phase extraction procedure. The eluate was collected into a 96-well plate and quantified by LC-MS/MS. The formation of M1 and M2 in the presence of inhibitors was compared with their formation in the absence of inhibitors. Negative control incubations were performed under similar conditions without HLM.

The recombinant human P450 enzyme, CYP1A2, CYP2A6, CYP2B6, CYP2C8, CYP2C9, CYP2C19, CYP2D6, CYP3A4, or CYP3A5 at 50 pmol/ml protein, was incubated with 3 μM compound I to identify the isoenzymes catalyzing the formation of M1 and M2. Incubation conditions and sample preparation were similar to those described above. Negative control incubation was carried out using microsomes from control Sf9 cells transfected with empty control vector. All incubations were conducted in triplicate.

Dosing and Sample Collection. A group of six noncannulated (three males and three females) Wistar Hanover rats were housed individually in stainless steel metabolism cages. A single dose of [^{14}C]compound I formulated as a solution in a vehicle of 0.5 M aqueous acetic acid was administered orally to intact rats (40 mg/kg). Urine was collected at 0 to 6, 6 to 12, and 12 to 24 h postdose and then at 24-h intervals through 168 h postdose. Feces was collected at 0 to 24 h postdose and then at 24-h intervals through 168 h postdose. In bile duct-cannulated rats, a single dose of [^{14}C]compound I was administered orally (four males and three females) at a dose level of 40 mg/kg. Urine was collected at 0 to 6, 6 to 24, and 24 to 48 h postdose. Feces were collected at 0 to 24 and 24 to 48 h postdose. Bile was collected at 0 to 3, 3 to 6, 6 to 12, 12 to 24, and 24 to 48 h postdose. In the circulation study, a single dose of [^{14}C]compound I was administered orally (seven males and seven females) at a dose level of 40 mg/kg. Blood was collected and processed for plasma at each of the following times, 0.5, 1, 3, 6, 12, 24, and 48 h postdose, from single animals of each sex. All samples were stored at −20°C before and after analysis.

For pharmacokinetic evaluation, individual animals (three males and three females) were given 40 mg/kg unlabeled compound I by gavage on the basis of body weight. Blood samples were collected via the tail vein at 0.5, 1, 3, 6, 8, and 24 h postdose. Plasma samples were prepared by centrifugation at 4°C for 10 min at 1500*g* within 30 min of blood sampling. Plasma was stored at −70°C before analysis.

Radioactivity Measurements. Radioactivity in urine and bile samples was analyzed directly by liquid scintillation counting on a Packard Tri-Carb liquid scintillation counter (Canberra Industries, Meriden, CT) by mixing Ultima Gold scintillation fluid (PerkinElmer Life and Analytical Sciences, Waltham, MA) to a known amount of the samples. Feces samples were homogenized in an approximately 1.5-fold volume of deionized water. Feces homogenates and blood were analyzed by solubilization. A suitable volume of solubilizing agent (Soluene-350) was added to samples. After an appropriate period (~1 h) of incubation at approximately 50°C, liquid scintillant was added before liquid scintillation counting. All radioassays were performed in at least duplicate.

Preparation of Urine, Bile, Feces, and Plasma Samples for Metabolite Profile Analysis. Urine from 0 to 24 h was pooled proportionally to the original sample volume collected at each time interval to obtain a representative pooled sample for each gender. Pooled rat urine samples were centrifuged at 10,000*g* for 10 min to remove debris and then a 50-μl aliquot of supernatant was injected onto the HPLC column for metabolite profile analysis.

Bile from 0 to 24 h was pooled proportionally to the original sample volume collected at each time interval to obtain a representative pooled sample. A 1-ml aliquot of pooled rat bile sample was mixed with 3 volumes of methanol-acetonitrile (v/v, 1:1) for protein precipitation and desalination. The pellet was washed with methanol-acetonitrile (v/v, 1:1). The solvent in the supernatant was evaporated to dryness under vacuum at 30°C for 4 h. The dry residues were reconstituted in 3 ml of water-acetonitrile (90:10) containing 0.05% formic acid. A 50-μl aliquot of reconstituted bile sample was injected onto the HPLC column for metabolite profile analysis.

Fecal homogenates from 0 to 48 h were pooled proportionally to original sample weights to obtain a representative pooled sample for each gender. Aliquots (5 ml) of pooled samples were centrifuged, and the supernatants were transferred to new vials. The fecal residues were extracted three times with 15 ml of methanol-water (80:20). The extracts were combined, and the solvent was reduced to approximately 200 μl under vacuum at 30°C. Then, water-acetonitrile (90:10) was added to the concentrated samples to restore the original sample volume of approximately 5 ml. After centrifugation, a 50-μl supernatant of each individual sample was injected onto the HPLC column for metabolite profile analysis.

Plasma samples were pooled in a time proportional manner to generate a 0 to 12 h representative pooled sample for each gender (Hamilton et al., 1981). A 1-ml aliquot of pooled plasma sample was mixed with 3 volumes of acetonitrile for protein precipitation. The solvent in the supernatant was evaporated to dryness under vacuum at 30°C for 4 h using an HT-4 series II centrifugal vacuum evaporator (Geneac Inc., Gardiner, NY). The dry residues were reconstituted in 0.2 ml of water-acetonitrile (90:10). A 50-μl aliquot of reconstituted plasma sample was injected onto the HPLC column for metabolite analysis.

Determination of Extraction Efficiency of ^{14}C-Labeled Compounds. To determine extraction efficiency of rat feces, homogenated fecal samples were accurately weighed (~1.0 g) and processed as described above. After reconstitution in 1.0 ml of methanol-water (80:20), the liquid was transferred to a scintillation vial along with 20 ml of scintillant and then analyzed by liquid scintillation counting. For plasma samples, an aliquot of pooled plasma was analyzed by liquid scintillation counting before extraction. After extraction, evaporation, and reconstitution, an aliquot of the processed plasma sample was analyzed using a liquid scintillation counter. The extraction efficiency was calculated by comparing the radioactivity of the processed sample with the radioactivity of unextracted samples analyzed as described above.

Preparation of Plasma Samples for Pharmacokinetic Evaluation. The plasma samples were extracted using protein precipitation. A 50-μl aliquot of plasma was mixed with 300 μl of internal standard (compound I-d_4) working solution in a 96-well plate and centrifuged at 650*g* for 5 min. A 10-μl aliquot of each supernatant was injected into the LC-MS/MS system for quantitative analysis.

HPLC-Radioactivity Analysis. Radiochromatographic analysis of samples from hepatocyte studies was performed on an Agilent 1100 system (Agilent Technologies, Santa Clara, CA). The separation was performed on a Synergi Hydro-RP column (4 μm, 4.6 × 150 mm; Phenomenex, Torrance, CA) at a flow rate of 1.0 ml/min. A binary solvent system was used in which solvent A was water with 23 mM ammonium formate (pH 3.5) and solvent B was acetonitrile. The analytes were eluted using the following gradient: a linear gradient from 5 to 15% B for first 15 min followed by a linear gradient to 19% solvent B over 17 min and a linear increase to 27% B over 6 min. The gradient was increased to 95% B by 45 min and held at that composition for 5 min, and then the mobile phase composition returned to the initial condition over 10 min. The HPLC elutant was split postcolumn at approximately a 1:9 ratio between the LTQ-Orbitrap mass spectrometer (Thermo Fisher Scientific) and a β-RAM model 3 radio flow detector (LabLogic, Broomhill, Sheffield, UK). The flow rate of IN-FLOW 2:1 liquid scintillation fluid (LabLogic) was 2 ml/min. The relative amounts of drug-related components in radiochromatograms are reported as a percentage of the total radioactivity (TRA) recovered during the HPLC run.

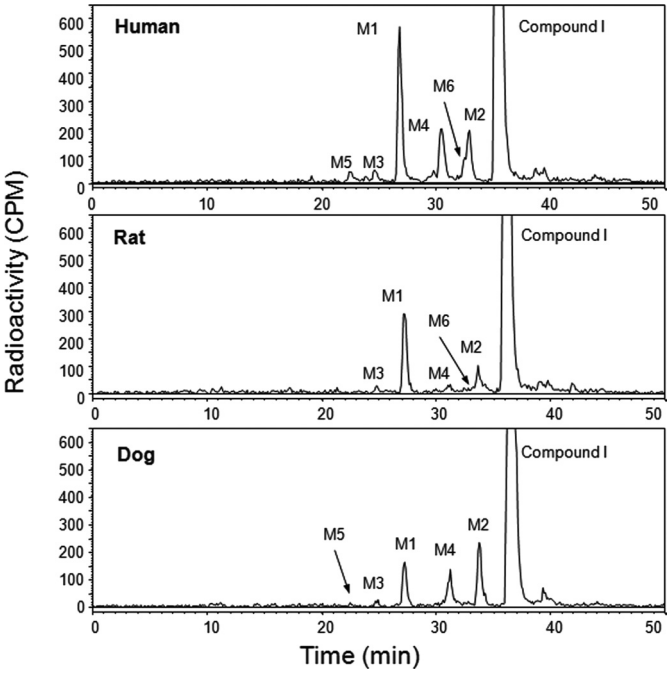

FIG. 2. Representative radioactivity profiles of [^{14}C]compound I metabolites in hepatocyte incubates.

Chromatographic analysis of samples from rat mass balance studies was performed on an Acquity UPLC system (Waters, Milford, MA). The separation was carried out on an Aquasil C18 column (4.6 × 150 mm, 5 μm; Thermo Fisher Scientific) at a flow rate of 1.0 ml/min. The mobile phase consisted of water with 20 mM ammonium formate (pH 3.0) (A) and acetonitrile (B). The analytes were eluted using the following gradient: 5% solvent B for 2 min, a linear increase to 25% solvent B over 23 min and maintained for 7 min, and a linear increase to 60% B over 7 min. The gradient was increased to 90% B for 5 min, and then the mobile phase composition was returned to the starting solvent mixture over 6 min. The HPLC elutant was split postcolumn at approximately a 1:9 ratio between the LTQ-Orbitrap mass spectrometer and a β-RAM model 3 radio flow detector. A 500-μl liquid scintillation cell was used in the radio flow detector. The flow rate of IN-FLOW 2:1 liquid scintillation fluid was 2 ml/min.

For plasma samples, HPLC eluates were split at approximately a 1:9 ratio between an LTQ-Orbitrap mass spectrometer and a HTS PAL fraction collector (LEAP Technologies, Carrboro, NC). The HPLC fractions were collected at the rate of 6.75 s/fraction into a total of six LumaPlate-96-well solid scintillator-coated microplates (PerkinElmer Life and Analytical Sciences) after each HPLC injection. The solvent in collected fractions was evaporated to dryness at room temperature. The radioactivities of collected plasma sample fractions were determined using a TopCount NXT microplate scintillation counter (PerkinElmer Life and Analytical Sciences, Waltham, MA) at a count time of 5 min.

LC-MS and LC-MS/MS Analysis. *Analysis of hepatocyte samples for metabolite identification.* Chromatographic separations were performed using the Acquity UPLC system described above. Mass spectrometric measurement was performed on a LTQ-Orbitrap XL mass spectrometer with electrospray ionization in positive ion mode. Data-dependent analysis was performed with full-scan data acquired at a resolving power of 30,000 in parallel with data-dependent collision-induced dissociation (CID) MS^n scanning triggered by a specific isotopic recognition pattern that was consistent with the ratio of unlabeled to ^{14}C-labeled parent drug used as substrates. The isotopic peak intensity ratio for triggering the dependent scan was set up at M:(M + 2) = 1:0.90(±0.14). CID product ion spectra of the three most intense ions matching the isotopic pattern were acquired within one acquisition cycle. Helium was used as the collision gas for CID. Normalized collision energies of 30 and 36% were set for CID MS^2 and MS^3, respectively.

Analysis of urine, bile, fecal, and plasma samples for metabolite identification. Chromatographic separations were performed using an HPLC system as described above. Data-dependent analysis was performed using an LTQ Orbitarp with full-scan data acquired at a resolving power of 15,000 in parallel with data-dependent CID MS^n scan mode. CID product ion spectra of the three most intense ions were acquired within one acquisition cycle. Helium was used as the collision gas for CID. Normalized collision energies of 30 and 35% were set for CID MS^2 and MS^3, respectively. All scan events were detected in the Fourier transform detector to give accurate mass data for precursor ions and MS^n ions used for metabolite identification.

Analysis of plasma samples for pharmacokinetics. Chromatography was performed on a Shimadzu LC-10AD system (Shimadzu, Kyoto, Japan). The separation was performed on a Sepax HP Silica analytical column (2.1 × 50 mm, 3-μm particle size; Sepax Technologies, Newark, DE) with a flow rate of 0.4 ml/min. The mobile phase consisted of (A) acetonitrile with 0.1% formic acid and 5 mM ammonium formate and (B) water with 0.1% formic acid and 5 mM ammonium formate. The analytes were eluted using a 3-min isocratic elution at an A/B ratio of 70:30. Positive tandem mass spectrometric analysis was performed with collision-induced dissociation and selective reaction mon-

TABLE 1

Mass spectra data and proposed structures of compound I metabolites in rat urine, bile, and feces

Metabolites	$[M + H]^{+a}$	$\Delta m/z$	MS^2 and MS^3 Product Ions[b]	Description of Metabolites	Samples
	Da	*ppm*			
M1	402.2166	2.5	MS^2: 385, 373, 345, 327, 319, 284, 270	N-Dealkylation	RH, DH, HH, RU, RF, RB
M2	485.2017	2.3	MS^2: 424, 387, 371, 359, 345, 284, 258	N-Demethylation	RH, DH, HH
M3	388.2026	1.6	MS^2: 371, 359, 331, 305, 270	N-Dealkylation	RH, DH, HH, RB
M4	513.1962	1.4	MS^2: 442, 424, 415, 387, 373, 298, 284, 258	Oxidation	RH, DH, HH, RF, RB
M5	416.1977	1.9	MS^2: 399, 387, 359, 327, 298	Oxidation and N-dealkylation	RH, DH, HH
M6	579.1743	2.2	MS^2: 499; MS^3: 424, 401, 385, 373, 359, 284	Sulfation	RH, DH, HH, RU, RF, RB
M7	418.2133	1.9	MS^2: 401, 389, 375, 363, 361, 343, 335	N-Dealkylation and hydroxylation	RU, RF, RB
M8	515.2125	2.7	MS^2: 440, 417, 389, 375, 373, 300, 274	Hydroxylation	RF, RB
M9	515.2120	1.7	MS^2: 440, 417, 389, 375, 300, 274	Hydroxylation	RU, RF, RB
M10	503.2491	3.1	MS^2: 446, 428, 389, 337, 370, 363, 361, 349, 323, 302	Hydrogenation	RF
M11	822.2964	1.8	MS^2: 411[c], 499, 402[c], 374[c], 347[c], 338[c], 329[c], 286[c]	GSH conjugation	RB
M12	691.2441	1.3	MS^2: 515; MS^3: 440, 417, 389, 375, 373, 300, 274	Hydroxylation and glucuronidation	RB
M13	840.3071	1.9	MS^2 (411[c]): 515, 497, 402[c], 308, 179	Hydroxylation and GSH conjugation	RB
M14	533.2227	1.9	MS^2: 458, 491, 440, 407, 419, 393, 389, 375, 318, 292	Hydroxylation and oxidation	RB
M15	691.2444	1.7	MS^2: 515; MS^3: 440, 417, 389, 375, 300, 274	Hydroxylation and glucuronidation	RU, RB
M16	545.2222	0.9	MS^2: 470, 431, 419, 405, 365 MS^3(419): 404, 362, 344, 318, 240	Oxidation and methylation	RB
M17	515.2125	2.7	$MS^{2:}$ 497, 417, 400, 385, 373, 319	N-Oxidation	RB

RH, rat hepatocytes; DH, dog hepatocytes; HH, human hepatocytes; RU, rat urine; RB, rat bile; RF, rat feces.
[a] Measured accurate mass of protonated molecule.
[b] Major or significant product ions.
[c] Doubly charged ion.

TABLE 2

Percentage of dose recovered in urine, feces, and bile from rats after oral administration of [^{14}C]compound I

Data are mean (SD).

Group	Radioactive Dose					
	Urine	Feces	Bile	Cage Rinse	Carcass	Overall Total
			%			
1						
Male (n = 3)	5.6 (1.3)	95.3 (3.6)	N.A.	0.6 (0.1)	0.3 (<0.1)	101.8 (3.8)
Female (n = 3)	8.9 (2.6)	90.4 (2.1)	N.A.	2.6 (2.7)	0.4 (0.1)	102.3 (3.6)
Mean (n = 6)	7.3 (2.6)	92.9 (3.5)	N.A.	1.6 (2.0)	0.4 (0.1)	102.2 (3.8)
2[a]						
Male (n = 4)	16.5 (4.7)	40.9 (6.5)	38.6 (4.4)	1.7 (0.7)	1.0 (0.4)	98.7 (1.3)
Female (n = 3)	17.0 (4.2)	46.6 (6.7)	30.6 (15.1)	3.5 (1.8)	1.9 (1.1)	99.5 (1.0)
Mean	16.8 (4.1)	43.3 (6.7)	35.2 (10.2)	2.4 (1.6)	1.4 (0.8)	99.1 (1.2)

N.A., not applicable.
[a] Bile duct-cannulated animals.

itoring on a Sciex API 3000 triple quadruple mass spectrometer (Applied Biosystems, Foster City, CA). The source temperature was 550°C, the electrospray was 4200 V, and the collision energy was 40. The ion transitions of m/z 499 to 155 for compound I and m/z 503 to 155 for the internal standard were monitored with a dwell times of 200 and 100 ms/transition, respectively.

Analysis of microsomal samples for identification of P450s. In enzyme identification studies, separation of compound I, M1, and M2 was performed with HPLC using a Phenomenex Onyx Monolithic Silica column (4.6 × 100 mm, 5 μm) connected to an HPLC system (Shimadzu, Columbia, MD). The eluting solvents consisted of 5 mM ammonium formate in 0.1% formic acid water (A) and 5 mM ammonium formate in 0.1% formic acid acetonitrile (B). The separation was performed under isocratic conditions over 4 min. The quantitative analysis was performed on a Sciex API 3000 triple quadrupole mass spectrometer using positive electrospray ionization in multiple reaction monitoring (MRM) mode. The MRM transitions of m/z 402.2 → 373.1 and 485.2 → 155.1 were measured for M1 and M2, respectively. M1-d_6 and M2-d_4 were used as internal standards and measured using MRM transitions of m/z 408.2 → 279.1 and 489.2 → 155.1, respectively.

Results

Extraction Efficiency. The mean extraction efficiencies for rat feces and plasma samples were 83 and 97%, respectively, suggesting that most of drug-related components were extracted during sample preparation.

Biotransformation Profiles in Hepatocytes. The representative radiochromatographic profiles from extracts of rat, dog, and human hepatocyte incubations are shown in Fig. 2. Unchanged compound I accounted for 48, 82, and 67% of the TRA, respectively, after incubation of 10 μM compound I with human, rat, and dog hepatocytes. A total of six metabolites of compound I were detected in hepatocytes from three species including five phase I metabolites (M1–M5) and a sulfate conjugate (M6) (Table 1). In rat and human hepatocytes, metabolite M1 generated via the loss of a thiazolylmethyl group was the most abundant metabolite, accounting for 9 and 23% of the TRA, respectively. Other major metabolites in human hepatocytes include an N-demethylated metabolite (M2) and a carboxylic acid metabolite (M4). Metabolite M2 was the predominant drug-related metabolite in dog hepatocytes. All the metabolites detected in human hepatocytes were also formed either in rat or dog hepatocytes. The structures of metabolites found in hepatocytes were interpreted along with metabolites detected in rats.

Excretion Profiles. The mean recoveries of radioactivity in urine and feces from bile duct-intact rats 5 days after oral administration of [^{14}C]compound I are summarized in Table 2. After oral administration, the mean overall recoveries of total radioactivity were 101.8 and 102.3% of the administered dose in male and female rats, respectively. The mean percentage of dose recovered in urine from male and female rats was approximately 5.6 and 8.9%, respectively. The mean percentage of dose recovered in feces from male and female rats was 95.3 and 90.4%, respectively. There was no sex-related difference in the route of excretion of [^{14}C]compound I.

In bile duct-cannulated rats, mean overall recovery of radioactivity was 99.2% after oral administration and mean excretion in feces, bile, and urine was 43.8, 34.6, and 16.8% of the administered dose, respectively. The radioactivity in urine and bile indicated that a minimum of 55.1% (males) or 47.6% (females) of the administered radioactivity was absorbed.

Radioactivity concentrations in blood and plasma of both male and female animals were characterized by peak levels occurring at 30 min. Concentrations of radioactivity in blood and plasma were similar at all sampling times, suggesting a rapid equilibration of drug-related material to the red blood cells.

Pharmacokinetic Analysis. The mean plasma concentrations versus time profile for unchanged compound I after a single 40 mg/kg oral dose were analyzed using a noncompartmental method (Table 3). The maximum plasma concentration (C_{max}) of compound I was 1.6-fold greater in female rats than in male rats. The mean exposure (area under the plasma concentration-time curve from 0 to 24 h) of compound I was slightly greater in female rats (27.6 $\mu M \cdot h^{-1}$) than male rats (20.2 $\mu M \cdot h^{-1}$). compound I was rapidly absorbed, and C_{max} was achieved within approximately 1 h (T_{max}) on average after oral administration. The mean terminal elimination half-life of compound I in male and female rats was approximately 3.3 and 2.1 h. respectively, also indicating that compound I was rapidly eliminated.

Metabolite Profiles in Rat. The representative radiochromatograms of rat feces after oral administration of [^{14}C]compound I are shown in Fig. 3. The most abundant phase I metabolites observed in rat feces were identified as an *N*-desthiazolylmethyl metabolite (M1) and a monohydroxylated metabolite (M9) that accounted for approximately 22 and 20% of total dosed radioactivity in male and female rats, respectively (Table 4). M6 was a sulfate conjugate (9% of dosed

TABLE 3

Mean pharmacokinetic parameters for compound I after a single 40 mg/kg oral dose of compound I

Animals	C_{max}	T_{max}	$t_{1/2}$	$AUC_{(0-24\ h)}$
	μM	h	h	$\mu M \cdot h^{-1}$
Male rats (n = 3)	4.0	1.5 (0.5–3)	3.3 (2.8–3.6)	20.2
Female rats (n = 3)	10.3	0.5 (–0.5)	2.1 (1.3–3.4)	27.6
Mean	7.2	1.0	2.7	23.8

C_{max}, maximum plasma concentration; T_{max}, time to reach maximum plasma concentration; $AUC_{0-24\ h}$, area under the plasma concentration-time curve from 0 to 24 h.

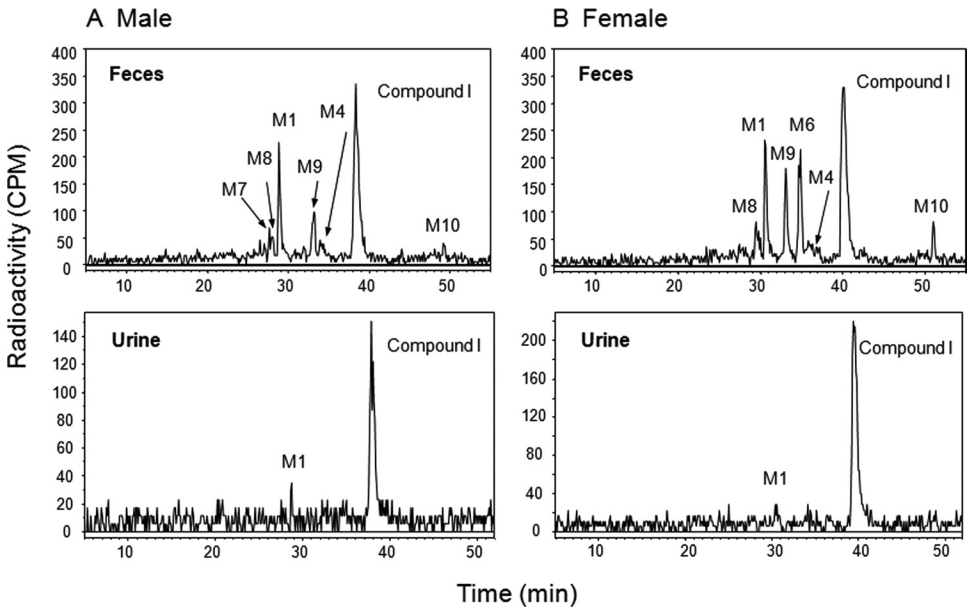

FIG. 3. Representative radioactivity profiles of [^{14}C]compound I metabolites in (A) feces (0–48 h) and urine (0–24 h) of male rats and (B) feces (0–48 h) and urine (0–24 h) of female rats after oral administration of a single 40 mg/kg dose of [^{14}C]compound I.

radioactivity) of compound I and was only detected in feces from female rats. M10 was a nonpolar component identified as a tetrahydroquinoline metabolite of compound I in rat feces.

Urinary metabolite profiles from bile duct-intact rats after oral administration of [^{14}C]compound I are shown in Fig. 3. The major component was [^{14}C]compound I with a trace amount of metabolite M1. Urinary metabolite profiles from BDC rats after an oral [^{14}C]compound I dose are shown in Fig. 4. Low levels of metabolites were detected, including phase I metabolites generated by N-dealkylation (M1), monooxidation (M9), combination of N-dealkylation or monooxidation (M7), and phase II metabolites formed by sulfation (M6) and glucuronidation (M15) that together accounted for 2.1 and 4.4% of the total drug-derived radioactivity in male and female rat, respectively.

The bile metabolite profile found in 0 to 24 h pooled bile after oral doses of [^{14}C]compound I in BDC rats is given in Fig. 4. Only a low level of unchanged compound I was detected in rat bile. Meanwhile, a much greater number of metabolites were detected in bile than that in rat urine or feces. The biliary metabolite profiles were similar between male and female rats except that M1 (the N-dealkylated metabolite) was the most abundant metabolite in male rats and accounted for 9.1% of the total dosed radioactivity, whereas M6 (a sulfate) was the most abundant metabolite in female rats and accounted for 11.7% of the total dosed radioactivity (Table 4). Other major metabolites observed in rat bile were oxidized metabolites (M7 and M9), sulfate (M6), GSH adducts (M11 and M13), and glucuronide conjugates (M12 and M15). Among them, M7 was only detected in bile from male rats. The hydrogenated metabolite (M10) observed in feces from BDC rat was not detected in the bile. No circulating metabolite of compound I was observed in rat plasma (Fig. 5).

Identification of Metabolites. On the basis of the radiochromatographic profiles of the metabolites in hepatocytes from three species

TABLE 4

Percentage of dose excreted over 24 h in urine, feces, and bile identified as compound I and its metabolites in male and female rats after a single oral dose of [^{14}C]compound I

Metabolite	Dose (Bile Duct-Intact Rats)				Dose (BDC Rats)			
	Feces		Urine		Bile		Urine	
	Male	Female	Male	Female	Male	Female	Male	Female
	%				%			
Compound I	55.9	44.1	5.0	8.2	1.0	1.3	13.9	11.2
M1	13.4	11.7	0.2	0.3	9.1	2.4	0.7	1.2
M3					3.3[a]			
M4	2.7				4.5	3.7		
M6		14.1			2.3	11.7		0.6
M7	2.8				3.3[a]		0.7	0.9
M8	2.6	4.3						
M9	8.6	8.8			2.4	2.3	0.7	1.3
M10	1.3	2.5						
M11					2.9	1.0		
M12					1.7	0.7		
M13					1.7	1.1		
M14					1.2	1.0		
M15					2.5	2.0		
M16					1.4	0.6		
M17					0.8			
Total	87.3	85.5	5.2	8.5	34.9	27.7	16.1	16.0

[a] In bile, M3 and M7 were not resolved.

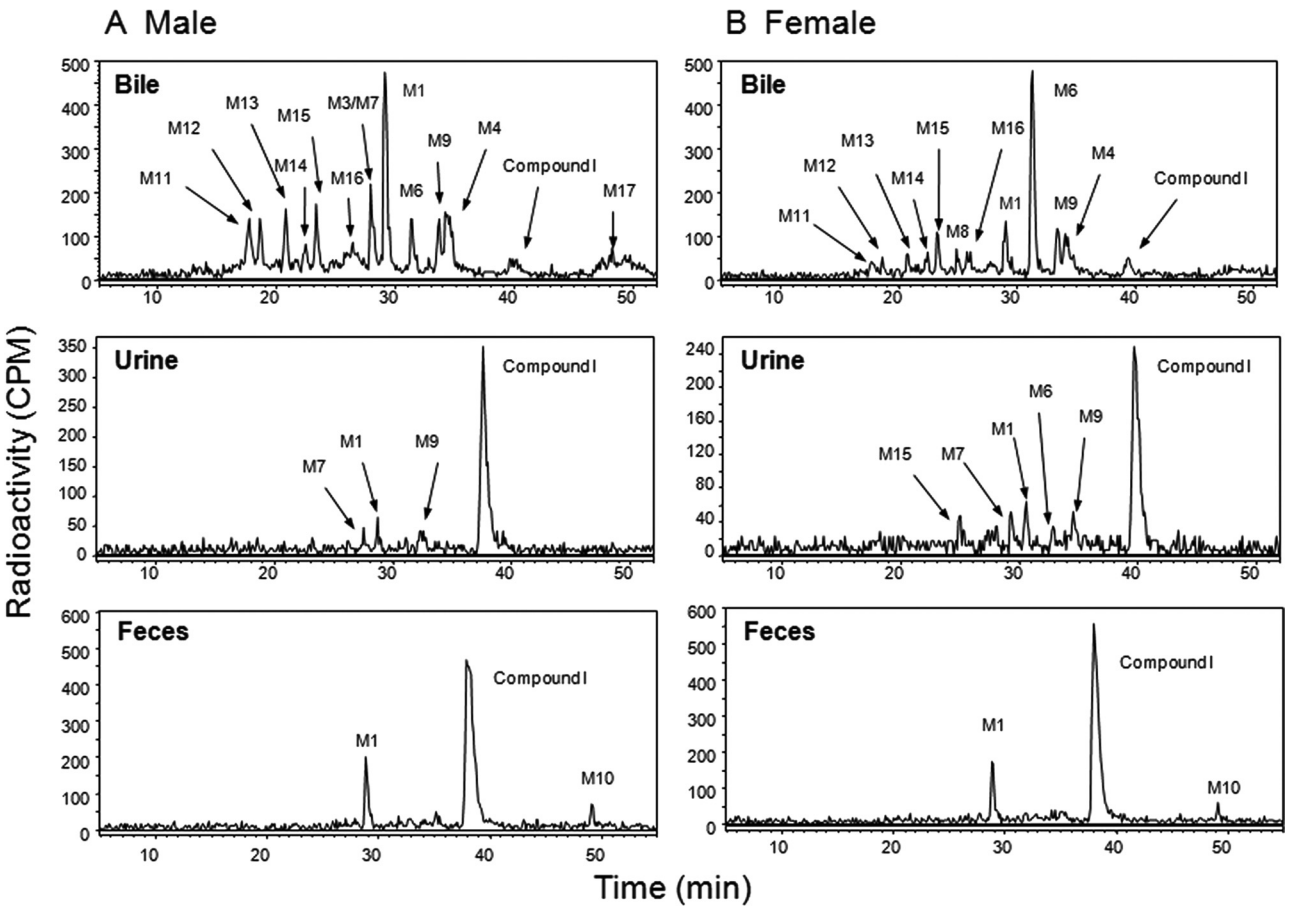

FIG. 4. Representative radioactivity profiles of compound I metabolites in BDC rats after oral administration of a single 40 mg/kg dose of [^{14}C]compound I. A, urine (0–24 h), bile (0–24 h), and feces (0–48 h) of male rats. B, urine (0–24 h), bile (0–24 h), and feces (0–48 h) of female rats.

and in vivo metabolites from rat, the structures of prominent metabolites were elucidated by high-resolution accurate mass spectrometry using isotopic pattern recognition, parent mass list, or intensity triggered data-dependent product ion scans on a LTQ-Orbitrap mass spectrometer. The fragment ions of compound I and its metabolites are shown in Table 1.

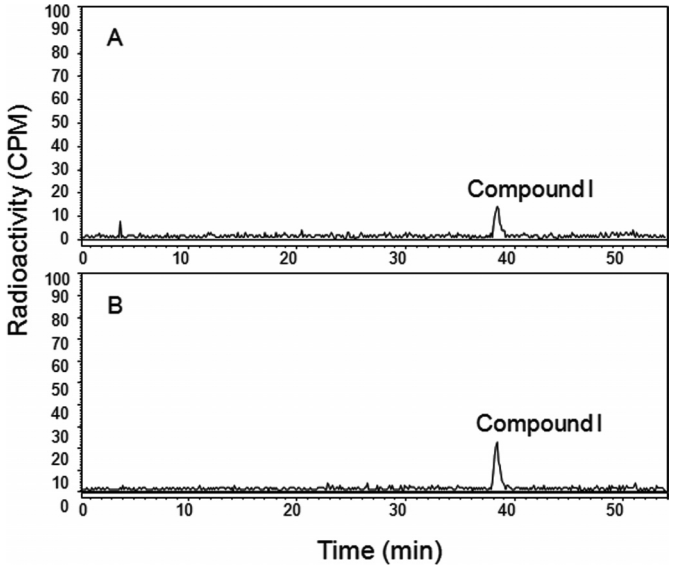

FIG. 5. Representative radioactivity profiles of [^{14}C]compound I metabolites in pooled plasma samples (0–24 h) from male (A) and female (B) rats after oral administration of a single 40 mg/kg dose of [^{14}C]compound I.

Compound I. The protonated molecule of compound I in the full-scan mode was at *m/z* 499. The base peak in the product ion spectrum was observed at *m/z* 373, associated with the cleavage of piperidine ring (Fig. 6A). Ions with lower abundance were detected at *m/z* 359, 401, and 424, corresponding to the cleavage of the piperidine ring, the loss of the *N*-thiazolylmethyl moiety, and the cleavage of the amide bond, respectively (Fig. 6A).

Metabolite M1. Metabolite M1 was one of the most abundant metabolites detected in vitro and in vivo. LC-MS scans of M1 showed a protonated molecule at *m/z* 402, 97 Da less than that of the parent drug. Accurate mass analysis of protonated M1 (observed at *m/z* 402.2166 within 2.5 ppm mass deviation of a calculated value) suggested that its empirical formula was $C_{25}H_{28}O_2N_3$ (equivalent to compound I − C_4H_3NS). The characteristic fragment ion at *m/z* 385 that resulted from the dissociation of the C–N bond of the piperidine ring was also observed in the mass spectrum of compound I, revealing that M1 was formed by the loss of the thiazolylmethyl moiety (Fig. 6B). Therefore, M1 was identified as *N*-(2-hydroxyethyl)-*N*-methyl-4-(piperidin-4-ylidene(quinolin-8-yl)methyl)benzamide. This conclusion was confirmed by comparing the retention time and product ion spectrum with those of an authentic synthetic standard.

Metabolite M2. LC-MS scans of M2 showed a protonated molecule at *m/z* 485, 14 Da less than that of the parent drug. Accurate mass analysis of protonated M2 (observed at *m/z* 485.2006 within 0.05 ppm mass deviation of a calculated value) suggested that its empirical

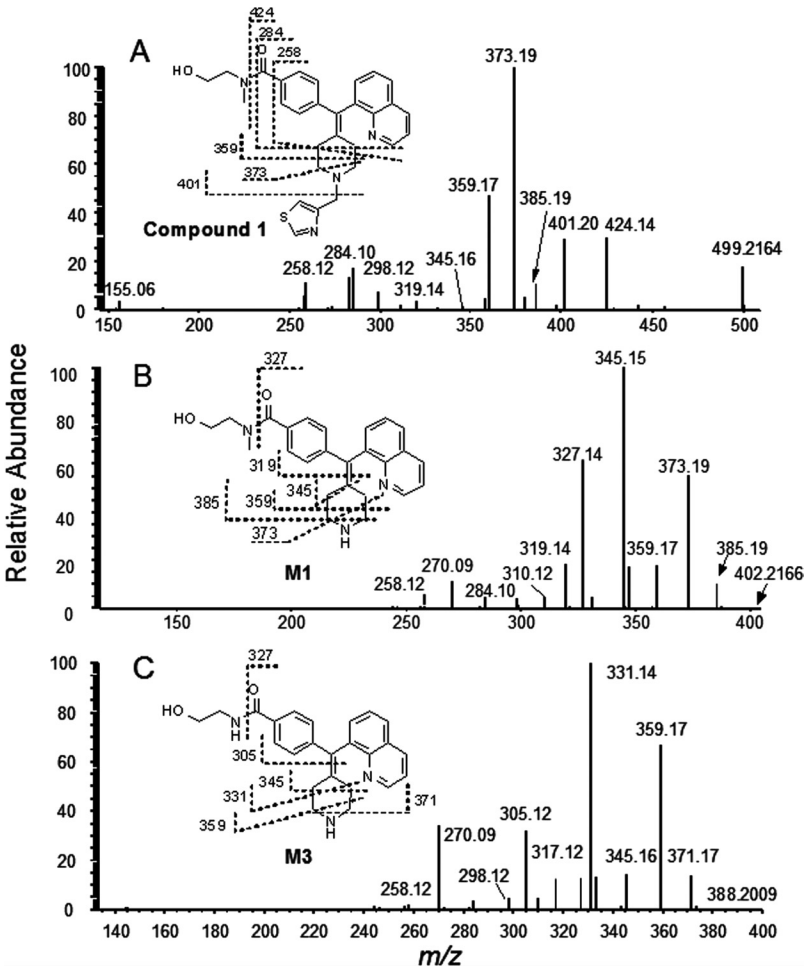

FIG. 6. CID product ion mass spectra of (A) compound I (MH^+ = 499), (B) M1 (MH^+ = 402), and (C) M3 (MH^+ = 388).

formula was $C_{28}H_{29}O_2N_4S$ (equivalent to compound I − CH_2) (Table 1). The diagnostic fragment ion at *m/z* 424 resulted from the dissociation of the amide bond, indicating that M2 was formed by the loss of a methyl moiety. Therefore, M2 was identified as *N*-(2-hydroxyethyl)-4-(quinolin-8-yl(1-(thiazol-4-ylmethyl)piperidin-4-ylidene)methyl) cyclohexa-1,3-dienecarboxamide. This conclusion was confirmed by comparing the retention time and product ion spectrum with those of an authentic synthetic standard (Fig. 1).

Metabolite M3. LC-MS scans of M3 showed a protonated molecule at *m/z* 388, 111 Da less than that of the parent drug. Accurate mass analysis of protonated M3 (observed at *m/z* 388.2025 within 1.6 ppm mass deviation of a calculated value) suggested that its empirical formula was $C_{24}H_{26}O_2N_3$ (equivalent to compound I − C_5H_5NS), also indicating the loss of a thiazolylmethyl moiety (− C_4H_3NS) (Fig. 6C). The high abundant fragment ions at *m/z* 359 and 331 generated by the cleavage of the piperidine ring together with a characteristic ion at *m/z* 327, resulting from dissociation of the amide bond indicated the loss of an *N*-methyl group from the benzamide side chain. Therefore, M3 was identified as *N*-(2-hydroxyethyl)-4-(piperidin-4-ylidene-(quinolin-8-yl)methyl)benzamide.

Metabolite M4. Metabolite M4 was detected in feces from bile duct-intact rats and bile from BDC rats. LC-MS scans of M4 showed a protonated molecule at *m/z* 513, 14 Da higher than that of the parent drug. Accurate mass analysis of protonated M4 (observed at *m/z* 513.1962 within 1.4 ppm mass deviation of a calculated value) suggested that its empirical formula was $C_{29}H_{29}N_4O_3S$ (equivalent to compound I − 2H + O). Compared with the spectrum of compound I, the fragment ions of M4 at *m/z* 373, 387, and 415 were 14 Da higher than the corresponding fragment ions of compound I, indicating that the oxygen was introduced into the moiety of 4-(quinolin-8-ylmethyl) benzamide (Table 1). Because the diagnostic ion at *m/z* 424 generated by the cleavage of the amide bond was also observed, it is plausible that oxidation occurred at the terminal carbon of the *N*-hydroxyethyl side chain to produce a carboxylic acid. Therefore, M4 was identified as 2-(*N*-methyl-4-(quinolin-8-yl(1-(thiazol-4-ylmethyl)piperidin-4-ylidene) methyl)benzamido)acetic acid.

Metabolite M5. LC-MS scans of M5 showed a protonated molecule at *m/z* 416, 83 Da less than that of the parent drug. Accurate mass analysis of protonated M5 (observed at *m/z* 416.1976 within 1.7 ppm mass deviation of a calculated value) suggested that its empirical formula was $C_{25}H_{26}O_3N_3$ (equivalent to compound I − C_4H_3NS − 2H + O), suggesting the loss of thiazolylmethyl moiety (Table 1). The base peak in the CID product ion spectrum of M5 was at *m/z* 327, which was also observed in the MS^2 spectrum of M3 generated by the dissociation of amide bond, suggesting that oxidation occurred on the benzamide side chain, and one oxygen was introduced. Based on these data, M5 was proposed as 2-(4-(piperidin-4-ylidene(quinolin-8-yl) methyl)benzamido)acetic acid.

Metabolite M6. LC-MS scans of M6 showed a protonated molecule at *m/z* 579, 80 Da higher than that of the parent drug, suggesting that M6 was a sulfate conjugate. Accurate mass analysis of protonated M6 (observed at *m/z* 579.1743 within 2.2 ppm mass deviation of a calculated value) gave its empirical formula as $C_{29}H_{31}N_4O_5S_2$. The MS^3 spectrum (579 → 499 →) of M6 was identical to the MS^2 spectrum of the parent drug. On the basis of these data, M6 was assigned as the *O*-sulfate of compound I.

Metabolite M7. Metabolite M7 was detected in feces from bile duct-intact rats and in urine and bile from bile duct-cannulated rats. M7 showed a protonated molecule at *m/z* 418, 81 Da less than that of the parent drug. Accurate mass analysis of protonated M7 (observed at *m/z* 418.2133 within 1.9 ppm mass deviation of a calculated value) suggested that its empirical formula was $C_{25}H_{28}N_3O_3$ (equivalent to compound I + O − C_4H_3NS), indicating that M7 was generated by the loss of the 4-methyl-1,3-thiazole moiety but addition of one oxygen atom to the parent drug (Table 1). The major fragment ions at *m/z* 343, 375, 389, and 401 were 16 Da higher than corresponding fragment ions of M1, indicating that M7 was a monohydroxylated *N*-desthiazolylmethyl metabolite of compound I, and hydroxylation occurred at the aromatic rings of 8-benzyl-quinoline. The exact location of hydroxylation could not be determined from the mass spectra.

Metabolites M8 and M9. Metabolite M8 was detected in rat bile. M8 showed a protonated molecule at *m/z* 515, 16 Da higher than that of the parent drug. The accurate mass of protonated M8 (observed at *m/z* 515.2125 within 2.7 ppm mass deviation of a calculated value) suggested that its empirical formula was $C_{29}H_{31}O_3N_4S$ (equivalent to compound I + O). The fragment ions at *m/z* 274, 300, 312, 375, 387, 417, and 440 were 16 Da higher than the corresponding fragment ions of compound I, indicating that M8 was a monohydroxylated metabolite of compound I and hydroxylation occurred at the aromatic rings of 8-benzyl-quinoline (Table 1). The exact location of hydroxylation could not be determined from the mass spectra. M9 was assumed be a regioisomer of M8 because of the same empirical formula and product ions (Table 1).

Metabolite M10. Metabolite M10 was only detected in feces from bile duct-intact rats and BDC rats. M10 displayed a protonated molecule at *m/z* 503, 4 Da higher than that of the parent drug. Accurate mass measurement of M10 gave a molecular ion at *m/z* 503.2491 and an empirical formula of $C_{29}H_{35}N_4O_2S$ (Δ = 3.1 ppm). The product ions at *m/z* 288, 302, 359, 377, 389, and 428 that were 16 Da higher

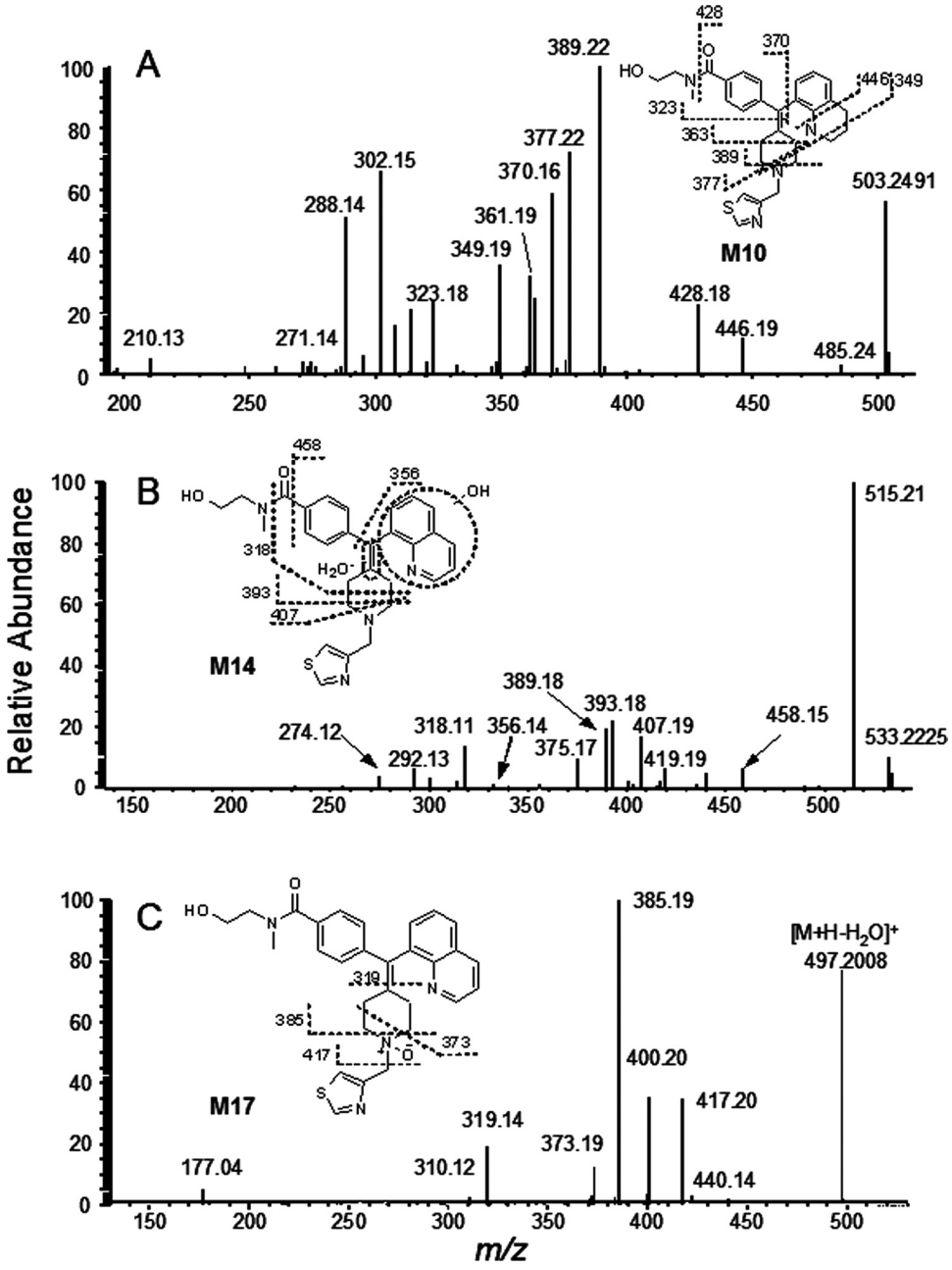

FIG. 7. CID product ion mass spectra of (A) M10 (MH^+ = 503), (B) M14 (MH^+ = 533), and (C) M17 (MH^+ = 515).

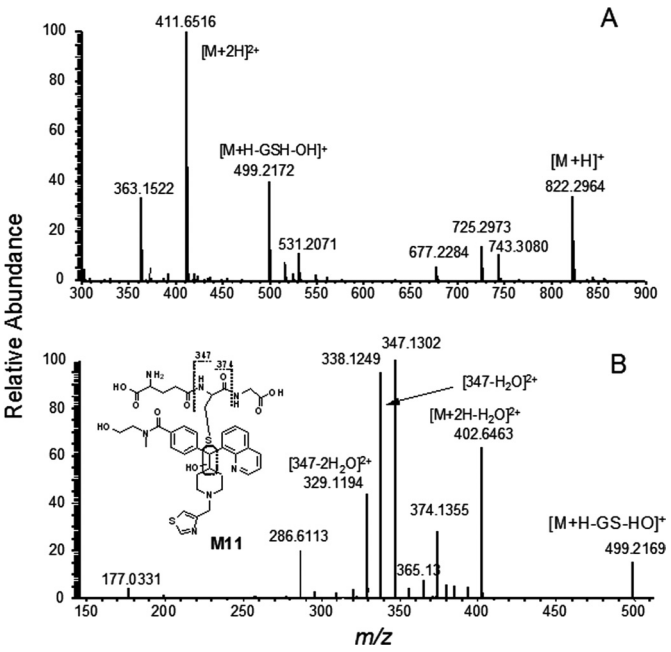

FIG. 8. CID product ion mass spectra of M11 ($MH^+ = 349$). A, MS^2 product ion spectrum. B, MS^3 product ion spectrum.

than corresponding fragment ions of compound I, together with a diagnostic fragment ion at *m/z* 370 (cleavage of bond between benzyl moiety and quinoline), indicated that four hydrogen atoms were introduced to the aromatic rings of quinoline (Fig. 7A). Furthermore, the characteristic fragments at *m/z* 446 and 349 resulting from the cleavage of quinoline revealed that the hydrogenation occurred at the quinoline ring, generating a 1,2,3,4-tetrahydro-quinoline. On the basis of these data, M10 was tentatively assigned as *N*-(2-hydroxyethyl)-*N*-methyl-4-((1,2,3,4-tetrahydroquinolin-8-yl)(1-(thiazol-4-ylmethyl) piperidin-4-ylidene)methyl) benzamide.

Metabolite M11. Metabolite M11 was detected in rat bile samples. M11 showed a protonated molecule at *m/z* 822, 323 Da higher than that of the parent compound (Fig. 8A). Accurate mass analysis of M11 gave a protonated molecular ion at *m/z* 822.2964 and an empirical formula of $C_{39}H_{48}N_7O_9S_2$ (Δ = 1.8 ppm) (equivalent to compound I + OH + glutathione). The MS^2 spectrum of the doubly charged ion at *m/z* 411.6 generated a typical ion at *m/z* 499.2 (a singly charged ion) that was associated with the parent drug, also suggesting that M11 is a GSH adduct generated by introducing one hydroxyl moiety and a −GS moiety to the parent drug directly (Fig. 8B). Theoretically, GSH and one oxygen atom could add on an exocyclic carbon-carbon double bond or a double bond of aromatic ring systems through an epoxide intermediate. However, if the addition of GSH and one oxygen atom occurred on a double bond of aromatic rings, the GSH adduct produced is not stable because of the breaking of aromaticity. In that case, the loss of water would be a high-priority step, generating an ion at *m/z* 804 instead of the ion at *m/z* 822, but this diagnostic ion at *m/z* 804 was not observed in the full-scan spectrum of M11 (Fig. 8A). Therefore, the most likely position for addition of a GSH moiety is on the exocyclic double bond rather than on aromatic rings. On the basis of these data, M11 was proposed to be a GSH adduct of compound I.

Metabolites M12 and M15. Metabolite M12 was detected in rat bile samples. M12 displayed a protonated molecule at *m/z* 691 or 192 Da higher than that of the parent compound (Table 5). The accurate mass of the protonated molecule was determined to be *m/z* 691.2441, corresponding to an empirical formula of $C_{35}H_{39}N_4O_9S$. The base peak in the CID product ion spectrum of M12 was at *m/z* 515, 176 Da less than that of the precursor ion, suggesting that M12 was a glucuronide conjugate. The accurate mass analysis of this base peak (observed at *m/z* 515.2114 with 0.5 ppm mass deviation of calculated mass) gave an empirical formula equivalent to $C_{29}H_{31}N_4O_3S$, one oxygen atom more than that of the parent drug. The MS^3 spectrum of M12 (691 → 515 →) was identical to the MS^2 spectrum of M8 or M9 (Table 1). On the basis of these data, M12 was assigned as an *O*-glucuronide conjugate of monohydroxylated compound I. M12 and M15 had the same empirical formula but a different HPLC retention time. MS^2 analysis of these two metabolites showed similar spectra, indicating that M12 and M15 are isomers because of the different positions of monohydroxylation on aromatic rings.

Metabolite M13. Metabolite M13 was detected in rat bile only. Its full-scan mass spectrum showed a protonated molecular ion at *m/z* 840, together with a doubly charged ion at *m/z* 411 and an ion at *m/z* 822 generated by the loss of water from the precursor ion. Accurate mass analysis of M13 gave a protonated molecular ion at *m/z* 840.3070 and an empirical formula of $C_{39}H_{50}N_7O_{10}S_2$ (Δ = 1.9 ppm) (equivalent to compound I + OH + GS + H_2O). The MS^2 spectrum of the doubly charged ion at *m/z* 411.6522 generated the typical ions at *m/z* 515.2123 (a singly charged ion) and 308.0911 (a protonated glutathione) (Table 1). The MS^3 spectrum (411.6 → 515 →) was identical to the MS^2 spectrum of M8/M9, suggesting that M13 was a GSH adduct and at least one hydroxyl group located at the benzylquinoline rings. Because the process of GSH conjugation might involve direct addition of GSH across the carbon-carbon double bond or the opening of a strained epoxide ring in multiple positions, the exact positions of hydroxylation and GSH addition could not be ascertained from the mass spectra.

Metabolite M14. Metabolite M14 was detected in rat bile samples. M14 showed a protonated molecule at *m/z* 533, 34 Da higher than that of compound I. Accurate mass measurement of M14 (observed at *m/z* 533.2227) suggested that its empirical formula was $C_{29}H_{33}N_4O_4S$ (Δ = 1.9 ppm). The characteristic fragment ions at *m/z* 318 and 458 generated by the cleavage of the amide bond and the C–C bond of piperidine revealed that M14 was formed by addition of a H_2O molecule and an oxygen atom to the exocyclic carbon-carbon double bond or the double bond on 8-benzylquinoline (Fig. 7B). Because the base peak of M14 in the MS^2 spectrum was at *m/z* 515 (equivalent to precursor ion − H_2O) and the MS^3 spectrum (*m/z* 533 → 515 →) was identical to that of M8 or M9, it is possible that the water molecule was introduced to the exocyclic double bond and the oxygen atom was introduced to the aromatic rings. In the MS^3 spectrum, the typical ion at *m/z* 356 associated with the loss of the benzylamide moiety indicated that the hydroxyl group was at the quinoline ring. The exact position of hydroxylation could not be ascertained from the mass spectra.

Metabolite M16. Metabolite M16 was detected in rat bile. LC-MS scans of M16 showed a protonated molecular ion at *m/z* 545, 46 Da higher than that of the parent drug. The accurate mass determination

TABLE 5

Enzymatic kinetics of compound I metabolism

	CYP2D6	CYP3A4	CYP3A5
M1			
V_{max} (pmol/min/mg)	1.0 ± 0.1	8.5 ± 0.2	5.8 ± 0.5
K_m (μM)	4.8 ± 1.2	9.3 ± 0.9	29.3 ± 6.4
Intrinsic clearance (μl/min/mg)	0.2	0.9	0.2
M2			
V_{max} (pmol/min/mg)	0.1 ± 0.01	1.4 ± 0.1	1.4 ± 0.04
K_m (μM)	22.0 ± 4.7	21.6 ± 3.0	16.4 ± 1.5
Intrinsic clearance (μl/min/mg)	<0.01	0.1	0.1

gave a protonated molecular ion at *m/z* 545.2222, providing the empirical formula $C_{30}H_{33}N_4O_4S$ (Δ = 0.9 ppm) (equivalent to compound I + O + OCH_2). The CID product ions at *m/z* 365 and 470 formed by the dissociation of the exocyclic double bond and amide bond, respectively, suggested that the oxygen atom and methoxyl group were introduced to benzylquinoline rings (Table 1). A characteristic fragment at *m/z* 240, resulting from the loss of benzylamide and the cleavage of the piperidine ring, was observed in the MS^3 spectrum (545 → 419 →), indicating that the hydroxylation and methoxylation occurred on the quinoline rings. The exact position of hydroxylation could not be ascertained from the mass spectra.

Metabolite M17. Metabolite M17 was detected in rat bile samples. The full-scan mass spectrum showed a protonated molecular ion at *m/z* 515 or 16 Da higher than that of the parent drug (*m/z* 499). The empirical formula of protonated M17 was determined to be $C_{29}H_{31}N_4O_3S$ by accurate mass measurement (equivalent to compound I + O). Compared with the CID spectrum of the parent drug, the product ions in the MS^2 spectrum at *m/z* 319, 373, and 417 suggested that one oxygen atom was introduced to the piperidine ring (Fig. 7C). In on-line H–D exchange experiments, only two active protons were replaced by deuterium, suggesting that the oxygen atom was directly connected to the amino group on the piperidine ring. Therefore, M17 was proposed to be an *N*-oxide metabolite.

Identification of Human P450 Enzymes Responsible for M1 and M2 Formation. Compound I was incubated with various human recombinant P450 enzymes to evaluate the contribution of individual enzymes to the formation of M1 and M2 (Fig. 9A). M1 formation was catalyzed most efficiently by recombinant CYP3A4 (2.3 pmol/min/pmol protein) followed by CYP3A5 (1.2 pmol/min/pmol protein) and CYP2D6 (0.6 pmol/min/pmol protein). CYP3A5 was the primary enzyme responsible for the M2 formation. CYP3A4 and CYP2D6 were also involved in producing detectable amounts of M2. Other recombinant cytochrome P450 enzymes and negative control incubation showed no activity in M1 or M2 formation. The formation of M1 and M2 in the presence or absence of selective inhibitors of cytochrome P450 in HLM was also evaluated to confirm the results from the assay using recombinant enzymes. Approximately 95% of M1 and M2 formation was inhibited by 1 μM ketoconazole, a selective CYP3A4/5 inhibitor (Fig. 9B), and less inhibition (83%) was observed at 0.2 μM ketoconazole for both M1 and M2. Other P450 inhibitors showed weak or no inhibitory effects on the production of M1 and M2 in human liver microsomes at high concentrations, and low inhibitor concentrations exhibited no inhibition on the formation of M1 or M2. The kinetics of the formation of M1 and M2 catalyzed by human CYP2D6, CYP3A4, and CYP3A5 were determined and are shown in Table 5. The kinetic parameters were calculated using nonlinear regression analysis to fit the data to the Michaelis-Menten equation. The results obtained from both recombinant enzymes and chemical inhibition assays clearly indicated that CYP3A4/5 are the major enzymes responsible for the formation of M1 and M2, and CYP2D6 might play a minor catalytic effect.

Discussion

To guide the selection of animal species for toxicology studies and address potential safety concerns, the metabolism of compound I was examined in rat, dog, and human hepatocytes in the current study. All the metabolites that were detected in human hepatocytes were also found either in rat or dog hepatocytes. M1, M2, and M4 were primary metabolites of [^{14}C]compound I across three species. Moreover, minor species differences were found in the in vitro incubations. In particular, *N*-dethiazolylmethyl metabolite (M1) was the most abundant metabolite in rat and human hepatocytes, whereas M2 was the most predominant metabolite in dog hepatocytes. The results suggest that rat and dog could be used as a model for toxicological safety assessments and for the prediction of the metabolic pathway of compound I in humans.

After a single oral dose of [^{14}C]compound I, most of the radioactivity was recovered in urine and feces by 24 h postdose. The total recovery of radioactivity was approximately 102.1% of the administered dose. The mean percentage of dose recovered in urine and feces from intact rats was 7.3 and 92.9%, respectively. In bile duct-cannulated rats, radioactivity was primarily excreted through feces (43.8% after oral dosing) and secondarily through bile (34.6% after oral dosing). Only a small portion (16%) of radioactivity was recovered in urine. These results together suggested that 1) compound I is excreted rapidly and almost completely within 24 h after dosing, 2) fecal excretion appears to be the major route for the elimination of metabolite and unchanged compound I in rats, and 3) the predominant parent-related component in the feces was the unchanged parent drug resulting from the unabsorbed portion of the oral dose. Given that the dose recovered in bile was 2-fold that in urine with a small portion of unchanged parent drug, hepatic metabolism played an important role in the elimination of absorbed compound I in rats.

After administration of the test substance, the percentage of the administered dose that is excreted via the bile and urine can be used to directly calculate the extent of oral absorption. In the current study, a minimum of 51% of administered dose was absorbed on the basis of the sum of radioactivity recovered in rat urine and bile from BDC rats. However, the recovered radioactivity in urine (~16%) from BDC rats was at least 2-fold that observed in urine (~7%) from intact rat,

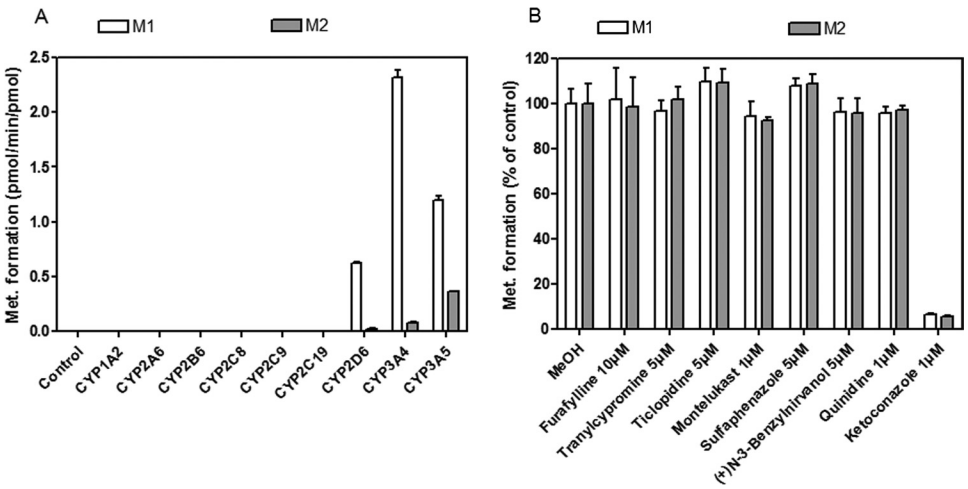

FIG. 9. Identification of specific P450 isoenzymes responsible for the formation of M1 and M2. A, rate of M1 and M2 formation by recombinant P450 isoenzymes. Recombinant human P450 enzymes were incubated with compound I (3 μM) at 37°C for 20 min in the presence of NADPH (1 mM). B, effects of selective chemical inhibitors of corresponding P450 isoenzymes on the formation of M1 and M2 in HLM. Control incubations were performed in the absence of chemical inhibitor.

indicating that bile duct ligation resulted in an increase in the urinary elimination of the parent drug-related components. This compensatory increase in urinary elimination after bile duct cannulation has been reported in other bioactive compounds (Wright and Line, 1980). Therefore, the discrepancy caused by bile duct cannulation should be considered when the data obtained in present study are used to estimate the fate of compound I in rodents.

Molecular weight is known to be another important factor affecting the degree of biliary elimination of certain compounds. It has been reported that the molecular weight threshold appears to be approximately 325 ± 50 for biliary excretion of polar compounds in rat (Hughes et al., 1973). In agreement with this report, compound I-derived metabolites (molecular weight ≥388) were mainly eliminated in rat bile. Even when the bile duct is obstructed, only a small amount of drug-related components was found in urine.

The identification of metabolites was achieved by accurate mass measurement and by analysis of their characteristic product ions. In addition to the parent drug, a total of 15 metabolites were observed by radiochemical detection and tentatively identified. The proposed scheme for the in vivo biotransformation of compound I is shown in Fig. 1. Most of the prominent metabolites found in rat and human hepatocytes were also observed in rats. The only exception is M2, which was not detected in BDC rats by radioactivity, suggesting that this route is relatively minor in vivo. The formation of the phase I metabolites in rats involved N-dealkylation (M1 and M3), oxidation on hydroxyethyl side chain (M4), aromatic hydroxylation (M8 and M9), N-oxidation (M17), and reduction (M10) (Fig. 9). Among them, M1 was a major metabolite observed in both bile and fecal samples from BDC rats, indicating that, except for liver enzymes, rat intestinal enzymes or bacteria are probably involved in producing the primary N-dealkylated metabolite. Moreover, metabolite M10 was only observed in rat feces from bile duct-intact or bile duct-cannulated rats, also revealing that only rat intestinal enzymes or gut bacteria catalyze the hydrogenation of the quinoline-ring to produce this reduced metabolite.

In summary, the results of this study provide information on in vitro biotransformation of compound I in hepatocytes from rat, dog, and human. The in vitro metabolite profiles of compound I in hepatocytes among the three species closely resembled each other. No human unique metabolite was observed. After single oral administration of [^{14}C]compound I to rat, the drug-related radioactivity was mainly eliminated via feces for which unchanged parent compound is the predominant component. The high proportion of radioactivity in the bile suggests that the biliary route plays an important role in the overall elimination of metabolites of compound I. The metabolite profiles of compound I in bile and urine showed that the primary biotransformation pathways of compound I in rats include N-dealkylation, oxidation, and sulfation. These metabolites were also observed in rat and human hepatocyte incubates, suggesting that rat was a suitable preclinical model for assessing safety. In addition, human liver CYP3A4/5 was identified as the primary enzyme responsible for the formation of the most abundant metabolites, M1 and M2, in liver. Given that CYP3A4 isoenzyme metabolizes more than 50% of all marketed pharmaceuticals (Guengerich, 1999), potential drug-drug interactions should be considered in clinical studies.

Acknowledgments

We thank Gary Moore, Valerie Hoesch, David Coomber, Mark E. Powell, Peter N. Dorff, Joan L. Morse, Dr. Eckhardt Schmidt, and other colleagues for their contributions to this study and Covance Laboratories (Harrogate, UK) for the conduct of the rat studies.

Authorship Contributions

Participated in research design: Guo, Gu, Zhou, Bui, and Grimm.

Conducted experiments: Guo, Gu, and Zhou.

Contributed new reagents or analytic tools: Elmore.

Performed data analysis: Guo, Gu, and Zhou.

Wrote or contributed to the writing of the manuscript: Guo, Gu, Zhou, Elmore, Bui, and Grimm.

References

Aguila B, Coulbault L, Boulouard M, Léveillé F, Davis A, Tóth G, Borsodi A, Balboni G, Salvadori S, Jauzac P, et al. (2007) In vitro and in vivo pharmacological profile of UFP-512, a novel selective δ-opioid receptor agonist; correlations between desensitization and tolerance. *Br J Pharmacol* **152:**1312–1324.

Bausch SB, Garland JP, and Yamada J (2005) The δ opioid receptor agonist, SNC80, has complex, dose-dependent effects on pilocarpine-induced seizures in Sprague-Dawley rats. *Brain Res* **1045:**38–44.

Broom DC, Jutkiewicz EM, Folk JE, Traynor JR, Rice KC, and Woods JH (2002) Nonpeptidic δ-opioid receptor agonists reduce immobility in the forced swim assay in rats. *Neuropsychopharmacology* **26:**744–755.

Burrows GD, Maguire KP, and Norman TR (1998) Antidepressant efficacy and tolerability of the selective norepinephrine reuptake inhibitor reboxetine: a review. *J Clin Psychiatry* **59 (Suppl 14):**4–7.

Filliol D, Ghozland S, Chluba J, Martin M, Matthes HW, Simonin F, Befort K, Gavériaux-Ruff C, Dierich A, LeMeur M, et al. (2000) Mice deficient for δ- and μ-opioid receptors exhibit opposing alterations of emotional responses. *Nat Genet* **25:**195–200.

Guengerich FP (1999) Cytochrome P-450 3A4: regulation and role in drug metabolism. *Annu Rev Pharmacol Toxicol* **39:**1–17.

Hajós M, Fleishaker JC, Filipiak-Reisner JK, Brown MT, and Wong EH (2004) The selective norepinephrine reuptake inhibitor antidepressant reboxetine: pharmacological and clinical profile. *CNS Drug Rev* **10:**23–44.

Hamilton RA, Garnett WR, and Kline BJ (1981) Determination of mean valproic acid serum level by assay of a single pooled sample. *Clin Pharmacol Ther* **29:**408–413.

Hughes RD, Millburn P, and Williams RT (1973) Molecular weight as a factor in the excretion of monoquaternary ammonium cations in the bile of the rat, rabbit and guinea pig. *Biochem J* **136:**967–978.

Jutkiewicz EM (2006) The antidepressant-like effects of δ-opioid receptor agonists. *Mol Interv* **6:**162–169.

Jutkiewicz EM, Torregrossa MM, Sobczyk-Kojiro K, Mosberg HI, Folk JE, Rice KC, Watson SJ, and Woods JH (2006) Behavioral and neurobiological effects of the enkephalinase inhibitor RB101 relative to its antidepressant effects. *Eur J Pharmacol* **531:**151–159.

Nieto MM, Guen SL, Kieffer BL, Roques BP, and Noble F (2005) Physiological control of emotion-related behaviors by endogenous enkephalins involves essentially the δ opioid receptors. *Neuroscience* **135:**305–313.

Papakostas GI, Stahl SM, Krishen A, Seifert CA, Tucker VL, Goodale EP, and Fava M (2008) Efficacy of bupropion and the selective serotonin reuptake inhibitors in the treatment of major depressive disorder with high levels of anxiety (anxious depression): a pooled analysis of 10 studies. *J Clin Psychiatry* **69:**1287–1292.

Perrine SA, Hoshaw BA, and Unterwald EM (2006) Delta opioid receptor ligands modulate anxiety-like behaviors in the rat. *Br J Pharmacol* **147:**864–872.

Raynor K, Kong H, Chen Y, Yasuda K, Yu L, Bell GI, and Reisine T (1994) Pharmacological characterization of the cloned κ-, δ-, and μ-opioid receptors. *Mol Pharmacol* **45:**330–334.

Saitoh A, Kimura Y, Suzuki T, Kawai K, Nagase H, and Kamei J (2004) Potential anxiolytic and antidepressant-like activities of SNC80, a selective delta-opioid agonist, in behavioral models in rodents. *J Pharmacol Sci* **95:**374–380.

Saitoh A, Yamada M, Yamada M, Takahashi K, Yamaguchi K, Murasawa H, Nakatani A, Tatsumi Y, Hirose N, and Kamei J (2008) Antidepressant-like effects of the delta-opioid receptor agonist SNC80 ([(+)-4-[(alpha*R*)-alpha-[(2*S*,5*R*)-2,5-dimethyl-4-(2-propenyl)-1-piperazinyl]-(3-methoxyphenyl)methyl]-*N*,*N*-diethylbenzamide) in an olfactory bulbectomized rat model. *Brain Res* **1208:**160–169.

Saitoh A, Yoshikawa Y, Onodera K, and Kamei J (2005) Role of δ-opioid receptor subtypes in anxiety-related behaviors in the elevated plus-maze in rats. *Psychopharmacology* (*Berl*) **182:**327–334.

Tejedor-Real P, Micó JA, Smadja C, Maldonado R, Roques BP, and Gilbert-Rahola J (1998) Involvement of α-opioid receptors in the effects induced by endogenous enkephalins on learned helplessness model. *Eur J Pharmacol* **354:**1–7.

Torregrossa MM, Jutkiewicz EM, Mosberg HI, Balboni G, Watson SJ, and Woods JH (2006) Peptidic delta opioid receptor agonists produce antidepressant-like effects in the forced swim test and regulate BDNF mRNA expression in rats. *Brain Res* **1069:**172–181.

Torregrossa MM, Isgor C, Folk JE, Rice KC, Watson SJ, and Woods JH (2004) The δ-opioid receptor agonist (+)BW373U86 regulates BDNF mRNA expression in rats. *Neuropsychopharmacology* **29:**649–659.

Vergura R, Balboni G, Spagnolo B, Gavioli E, Lambert DG, McDonald J, Trapella C, Lazarus LH, Regoli D, Guerrini R, et al. (2008) Anxiolytic- and antidepressant-like activities of H-Dmt-Tic-NH-CH(CH_2-COOH)-Bid (UFP-512), a novel selective δ opioid receptor agonist. *Peptides* **29:**93–103.

Wright WE and Line VD (1980) Biliary excretion of cephalosporins in rats: influence of molecular weight. *Antimicrob Agents Chemother* **17:**842–846.

Address correspondence to: Dr. Jian Guo, Clinical Pharmacology & DMPK, AstraZeneca Pharmaceuticals, 1800 Concord Pike, Wilmington, DE 19803. E-mail: jian.guo@astrazeneca.com